ISSN 1070-3284, Russian Journal of Coordination Chemistry, 2019, Vol. 45, No. 11, pp. 817–823. © Pleiades Publishing, Ltd., 2019.

A New Coordination Polymer for Effective 5-Fluorouracil Loading and Anti-Lung Cancer Activity Study

L. Y. Shi[a], W. Zhang[b], G. Z. Zhou[c], and Q. Cao[b, *]

[a]*Department of Respiratory and Critical Care Medicine, Affiliated Baoji Hospital of Xi'an Medical University, Baoji, Shaanxi, P.R. China*

[b]*The Affiliated Hospital of Yan'An University, Yan'An, Shaanxi, P.R. China*

[c]*Respiratory Department of Ankang Traditional Chinese Medicine Hospital, Ankang, Shaanxi, P.R. China*

******e-mail: qiang_cao666@aliyun.com*

Received June 27, 2018; revised October 31, 2018; accepted November 24, 2018

Abstract—A new three-dimensional porous coordination polymer with the formula of [Ba(HTATB)-(H_2O)]$(DMF)_2$ (**I**) has been solvothermally synthesized from 4,4',4"-s-triazine-2,4,6-triyltribenzoic acid (H_3TATB) and $Ba(NO_3)_2$ under DMF media and characterized by single crystal X-ray diffraction (CIF file CCDC no. 1856562) and elemental analysis. The efficient encapsulation of an anticancer drug 5-fluorouracil (5-FU) on the desolvated **I** (**Ia**) has been studied both experimentally and computationally. In addition, in vitro anti-lung cancer activity of compounds **I** and 5-FU loaded 1a have also been evaluated using MTT assay.

Keywords: three-dimensional, encapsulation, X-ray, anti-liver cancer activity

DOI: 10.1134/S1070328419110083

INTRODUCTION

Cancer is a threat to the health of human beings that causes millions of deaths annually [1]. Chemotherapy is still the dominant treatment method [2]. However, traditional direct administration of therapeutic drugs to patients is no longer applicable due to intrinsic limitations, including undesirable side effects, poor pharmacokinetics and poor biodistribution [3]. Thus, various efforts have been made toward the development of drug vehicles for controllable drug release that achieve reduced side effects and enhanced therapeutic efficacy.

Coordination polymers are crystalline materials composed of metal ions, connected by functionalized organic linkers, forming a hierarchy of structure [4–6]. A wide variety of metal centres and functionalized organic linkers are used to form MOFs under different synthetic conditions, giving rise to unprecedented structural diversity tailored for specific application [7–9]. Recent studies have shown that the porous coordination polymers have demonstrated great potential in the biomedical fields such as drug delivery [10]. To achieve the requirements of desirable drug carriers, the corresponding biocompatibility should be considered. Although some coordination polymers could house a large capacity of drug molecules, their metal centers, such as Cr^{3+}, Cd^{2+} and Ni^{2+} are highly toxic to the human beings. In this work, concerning cytotoxicity of the drug carrier, we adopt the nontoxic metal cation Ba^{2+} and an organic carboxylic ligand 4,4',4"-s-triazine-2,4,6-triyltribenzoic acid (H_3TATB) to construct a new three-dimensional Ba(II)-based coordination polymer, namely [Ba(HTATB)(H_2O)]$(DMF)_2$ (**I**) by reaction of $Ba(NO_3)_2$ and H_3TATB in a mixed solvent of *N*,*N*'-dimethylacetamide (DMF) and H_2O at 120°C under solvothermal condition. The structure of this compound is determined by singe-crystal X-ray diffraction and elemental analysis. We use the grand canonical ensemble Monte Carlo (GCMC) simulation to probe the sorption performance of the solvent-free **I** toward the anticancer 5-fluorouracil (5-FU), which shows that this coordination polymer could take up considerable amount of 5-FU with a moderate strong framework-guest interaction. Finally, the two compounds (**I** and 5-FU loaded **Ia**) in vitro anti-lung cancer was then evaluated on two human lung cancer cells (A549 and NCI-H1299).

EXPERIMENTAL

Apparatus and materials. All the starting materials and reagents used in this work were obtained commercially and used without further purification. Element analyses (C, H, and N) were determined with an elemental Vairo EL III analyzer. Powder X-ray diffraction (PXRD) data were collected using PANalytical X'Pert Pro powder diffractometer with CuK_α radiation and $5° \le 2\theta \le 50°$.

Synthesis of I. A mixture of 0.052 g (0.2 mmol) of $Ba(NO_3)_2$ and 0.087 g (0.2 mmol) of H_3TATB were

weighed in a clean glass vial and dissolved in 10 mL of DMF. The mixture was sonicated and then kept in an oven at 100°C for 120 h. Colorless crystals of **I** were collected (in a yield of 76% with respect to the ligand) and washed with DMF.

For $C_{30}H_{29}N_5O_9Ba$ (**I**)

Anal. calcd., %	C, 48.63	H, 3.95	N, 9.45
Found, %	C, 48.51	H, 3.69	N, 9.26

The activated **I** (**Ia**) was prepared by soaking the crystalline samples of **I** in MeOH for three days (fresh MeOH was replaced in each 12 h) and then pumped under high vacuum for one day at 80°C.

Crystal structure determination. Suitable single crystal of compound **I** was carefully selected under optical microscope and glued on thin glass fibers. The intensity data of **I** was collected on Oxford Xcalibur E diffractometer. The empirical absorption corrections were applied to the data using the SADABS system. This structure was solved by direct method and refined by full-matrix least-squares method on F^2 using the SHELXS-97 program. All non-hydrogen atoms of **I** were refined anistropically, and all the hydrogen atoms attached to carbon atoms were fixed at their ideal positions. Crystal data for $C_{30}H_{29}N_5O_9Ba$: orthorhombic, space group $Pna2_1$, $a = 7.3344(2)$, $b = 19.3892(7)$, $c = 26.2341(10)$ Å, $V = 3730.7(2)$ Å^3, $Z = 4$, $T = 293(2)$ K, $\mu(MoK_\alpha) = 1.096$ mm^{-1}, $\rho_{calcd} = 1.055$ g/cm^3, 12039 reflections measured ($5.938° \le 2\theta \le 49.996°$), 5692 unique ($R_{int} = 0.0415$, $R_{sigma} = 0.0580$) which were used in all calculations. The final R_1 was 0.0429 ($I > 2\sigma(I)$) and wR_2 was 0.1076 (all data).

Supplementary material for structure **I** has been deposited with the Cambridge Crystallographic Data Centre (no. 1856562; deposit@ccdc.cam.ac.uk or http://www.ccdc.cam.ac.uk).

Computational details. In order to assess the adsorption behavior of 5-FU on **I**, GCMC simulations were performed to calculate the adsorption isotherms and heats of pure components in MOFs with the Material Studio 8.0. In this work, we used the all atom models for 5-FU and **I** and their charges are calculated by the Qeq method. The intermolecular interactions for different sites were described by a Lennard-Jones (LJ) plus coulombic potential. The model of **I** was constructed from the X-ray diffraction (XRD) data while the model of 5-FU was acquired though the MM calculation. We used the UFF force field to model the atoms of **I** and 5-FU. The favorable binding site was delivered from the fixed loading task and the distributing sites were obtained from the fixed pressure task in the sorption model.

Antitumor activity. Two human lung cancer cells (A549 and NCI-H1299) and one human normal cells were grown in a RPMI 1460 medium supplemented with 10% fetal calf serum, 100 μg/mL penicillin and 100 μg/mL streptomycin. They were incubated at the temperature of 37°C in a moist incubator and 95% air and 5% CO_2. Cells at the exponential growth were diluted to 5×10^4 cells/mL with RPMI1640, and then seeded in 96-well cell culture at a volume of 100 μL per cell, respectively, and incubated for 24 h at 37°C in 5% CO_2. After incubation of cells for up to 96 h, medium was removed from each cell and 150 μL of MTT (0.5 mg/mL) solution, diluted 10-fold by RPMI 1460 was subsequently added. The IC_{50} values were measured by depicting the ratio viability versus concentration on a logarithmic chart and reading off the concentration where 50% of cells viable involved in the control. In order to get the mean values, it is requested that each experiment was conducted at least three times in the same way.

RESULTS AND DISCUSSION

The title complex **I** could be obtained via an one pot solvothermal reaction of H_3TATB and $Ba(NO_3)_2$ in a mixed solvent of DMF and water at 120°C. Asymmetric unit of **I** contains one Ba^{2+} ion, one of $HTATB^{2-}$ ligand and one coordinated water molecule. The Ba(1) ion connected to nine oxygen atoms (one coordinated water and eight carboxylic O atoms) to form the BaO(9) polyhedral unit with a distorted single capped square-antiprism geometry as calculated via the shape software (Fig. 1a). The Ba–O bond lengths are in the range of 2.753(2)–2.959(4) Å, which are comparable with other Ba-based coordination polymers reported in the literature [11–15]. The Ba^{2+} ions are linked through oxygen atoms edge-wise to form a one-dimensional chain with infinite Ba–O–Ba bonds along the *a* axis. Only one type of $HTATB^{2-}$ anion is present in the molecular unit, and it uses its three carboxylic groups to connect with six different Ba^{2+} ions; the bonding connectivity allows one of the oxygen atoms to be free (Fig. 1b). The connectivity in **I** between the Ba^{2+} ions and $HTATB^{2-}$ anions gives rise to a neutral three-dimensional structure. One-dimensional chains are connected to six other chains through $HTATB^{2-}$ anions forming a three-dimensional architecture with (6)-net connectivity. This connectivity creates one-dimensional channels along the *a* axis. Due to the C(3) symmetry and mutual stacking of the $HTATB^{2-}$ ligands, the one-dimensional channels take the shape of distorted honeycombs. The dimensions of the channels are approximately 10×15 Å^2, and the channels are occupied by lattice DMF and water molecules (Fig. 1c). The coordinated water molecules are directed toward the pore interior. The guest-accessible void volume, as calculated by PLATON software, is 31%. Topological analysis using TOPOS software identified that the structure has a 6/4/o4-type topological network with a uninodal 6-c net, which can be presented as the Schläfli

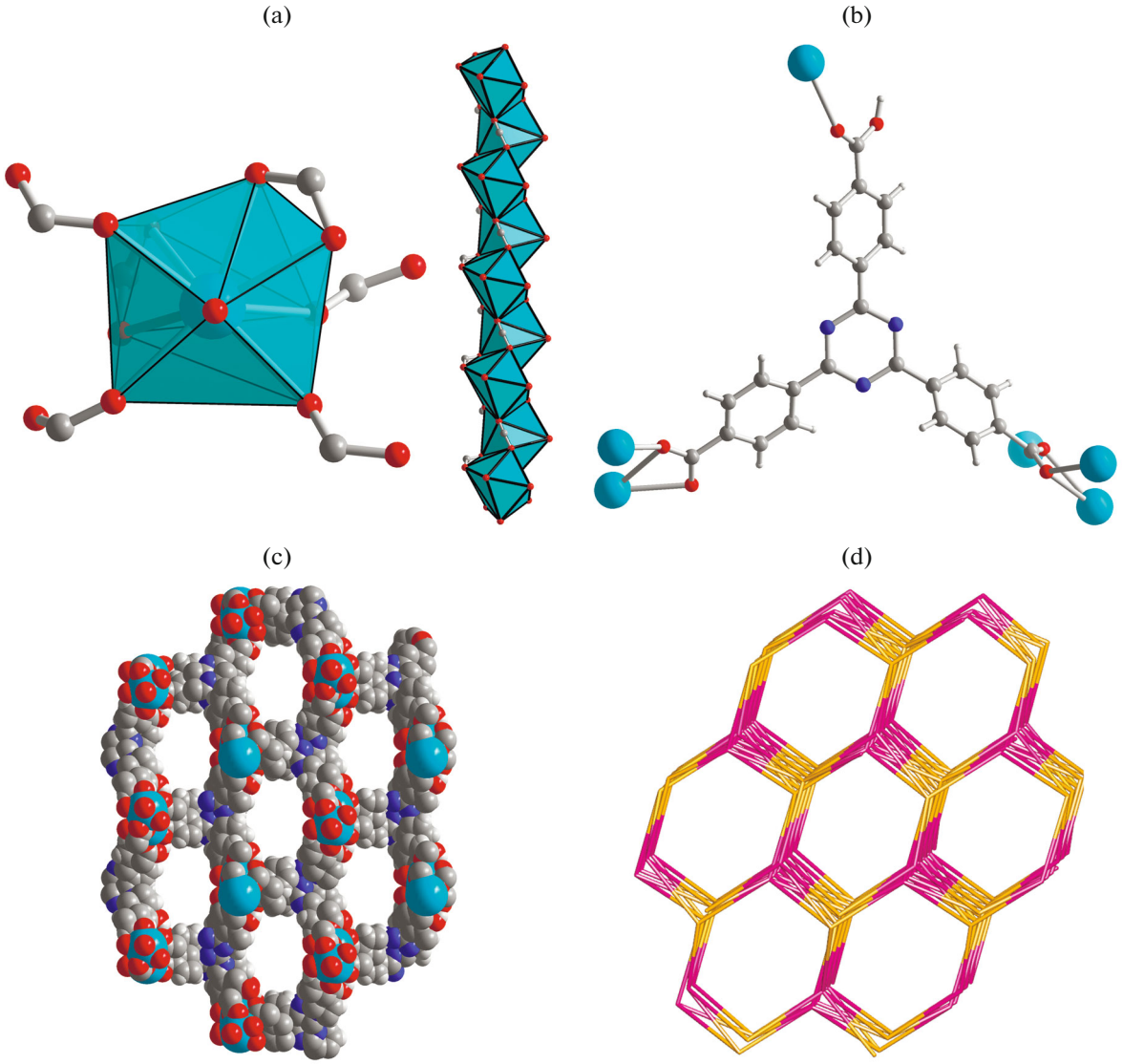

Fig. 1. View for the coordination surroundings for the Ba atoms in **I** (a); view for the connection modes for the $HTATB^{2-}$ ligands of **I** (b); view for the one-dimensional channels of I (c); the 6/4/o4-type topological network for **I** (d).

symbol {4^9.6^6} (Fig. 1d). It should be mentioned that although the structure of **I** is isostructural to the Ba(II)-coordination polymers composed of 1,3,5-benzenetribenzoic acid ligand in the literature, most of the reported ones show anionic network structures with the Me_2NH_2 cations occupying the free spaces [11–13]. The potential solvent accessible free voids and the uncoordinated N atom sites in the channels make compound **I** a promising vessel for guests' accommodation.

The PXRD pattern of the as-synthesized **I** was collected at room temperature, and the good agreement with its simulated pattern confirms its high phase purity (Fig. 2a). The TGA curve of **I** shows a continuous weight loss of 22.4% from room temperature to 446°C (calcd. 22.1%), which could be attributed to the loss of one coordinated water and two lattice DMF molecules (Fig. 2b). After a short plateau till 517°C, the framework of **I** begins to collapse. The morphology of the as-prepared samples of **I** was also probed via the scanning electron microscopy (SEM), which reveals their block-shape crystalline products with the average size of 80 μm (Fig. 2c). The single crystal structure showed that compound **I** is microporous in nature, which prompted us to measure the porosity of the activated compound **I**. Before the gas sorption study, about 80 mg of crystalline compound **I** was soaked in MeOH for three days and then pumped under high vacuum for one day at 80°C to afford the activated **I** (denoted as **Ia** hereafter). The PXRD pat-

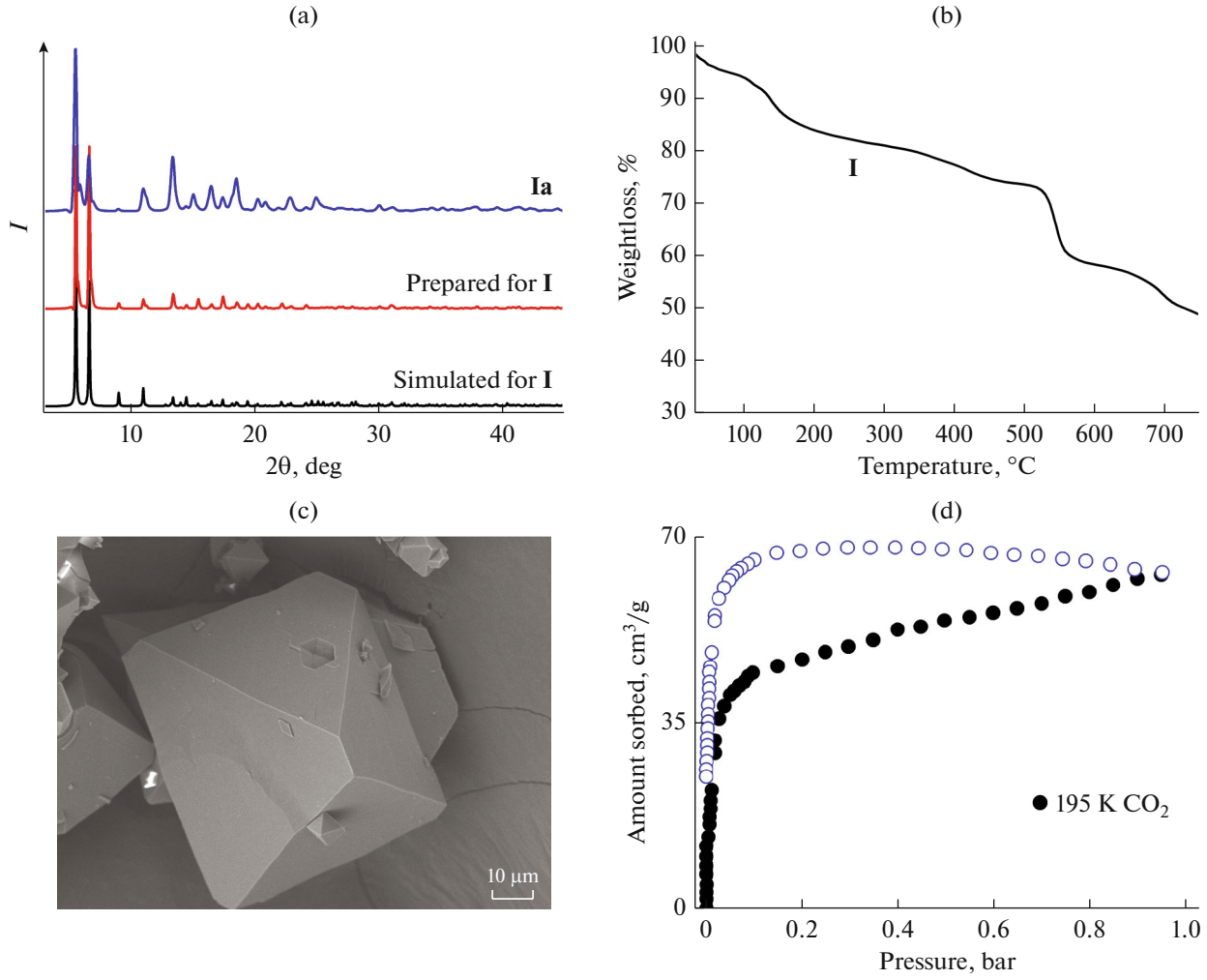

Fig. 2. The PXRD patterns of **I** and **Ia** (a); the TGA curve of **I** (b); the SEM image for **I** (d); the CO_2 sorption data for the activated **I** at 195 K: adsorption points (black), desorption points (blue) (c).

tern of **Ia** matches well with that of **I**, indicating the framework integrity is kept in the activation process (Fig. 2a). CO_2 adsorption at 195 K showed a type-I isotherm and confirmed the robust porosity via the reversible isotherm. The Brunner–Emmet–Teller (BET) surface area was calculated to be 320 m^2/g (Fig. 2d). It could be noticed that there is an increasing trend for the CO_2 desorption isotherm upon lowing the pressure, which might be due to the multidimensional micropores in **Ia** making the gas escape from the pores difficult at high press. When the pressure is lower, the gas suddenly escapes in a large amount from the pores, thus, leads to the increase of amount of CO_2 desorption isotherm. Similar increasing trend of desorption isotherm has been observed in the reported literature [16, 17].

As discussed above, the title complex **I** has considerable solvent accessible free volume and water occupied metal sites, which indicates that it could serve as a good drug carrier for the anticancer drug 5-FU. More importantly, compared with other toxic MOFs, such as Cd-MOFs and Cr-MOFs, the Ba-MOF reported here is more environment-friendly and biocompatible. The drug-loading capacity of the activated **I** was evaluated by impregnating the samples in 5 mL solution containing 5-FU (30 mg) with stirring, and investigated the encapsulation of 5-FU into them by UV-Vis spectroscopy. The entry of 5-FU into the framework of **I** leads to the decrease of adsorption intensity obviously. The loading amount was determined by UV-Vis spectroscopy at 254 nm and the result showed 34.32 wt % 5-FU uptakes. Drug release experiments were taken by dialyzing the drug-loaded **I** in the PBS buffer solution (PBS = phosphate buffered

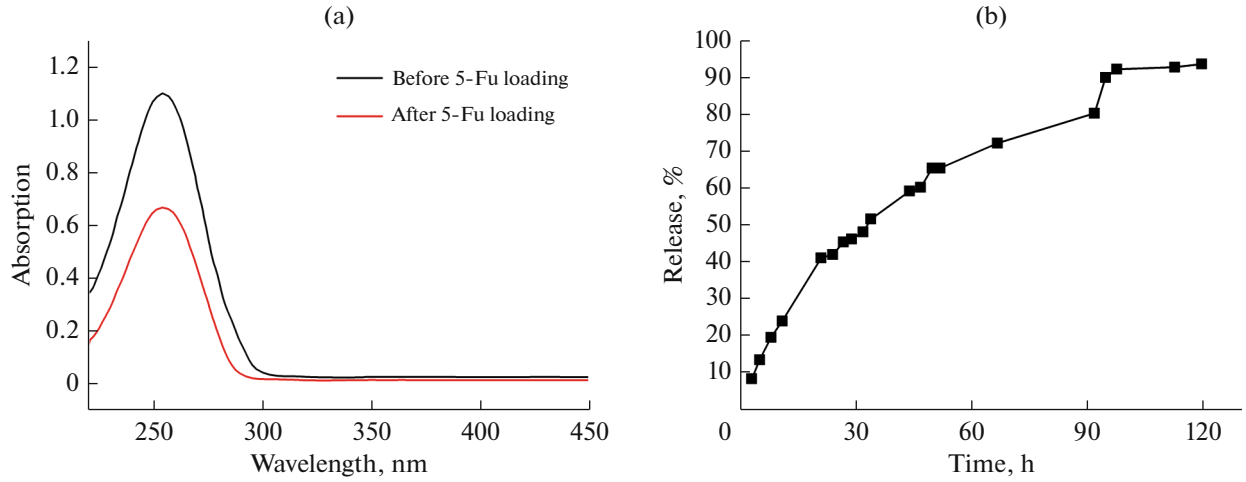

Fig. 3. The UV-Vis spectroscopy for the 5-FU–MeOH solution before and after 5-Fu loading (a); the release process of 5-FU from the drug-loaded **I** (%5-FU vs. time) (b).

saline pH 7.4) at 37°C. The delivery of 5-FU occurred within a week and 92% of the loaded drug was released (Fig. 3). 5-FU loaded **I** exhibits a slow release in PBS and approximately 50% of the drug was released at the early stage (30 h), then, a more stable release of smaller dosage occurred for one day. After 72 h, a much-burst release curve generates up to 10 h. The hydrogen bonded interactions between 5-FU and the organic ligand may lead to this slow release.

To gain a more deep understand of the 5-FU loading process in the complex **I**, we performed configurational bias Monte Carlo (CBMC) and molecular dynamics (MD) simulations to compute the adsorption and diffusion of 5-FU molecules in the framework of **I**. We initially performed CBMC simulations using the fixed pressure task in the sorption module of Materials Studio 8.0 to determine the adsorbed number of 5-FU molecules in **I** at 1 bar and room temperature. As shown in Fig. 4a, the simulation result indicates that the activated **I** could uptake 17 5-FU molecules per four-unit cells, corresponding to 32.4 wt % (~0.26 g/g), which is comparable with those porous MOFs targeted for the 5-FU delivery. Furthermore, the 5-FU molecules could from H-bond interactions with the N atoms and O atoms on the $HTATB^{2-}$ ligand, which are very important for slowing down the drug releasing rate, leading to the drug sustained release. The density distribution also shows that the 5-FU molecules mainly locate near the N atoms and the undeprotonated carboxylic O atom on the $HTATB^{2-}$ ligands, indicating the importance of H-bond interaction for the accommodating 5-FU molecules in the framework of **I** (Fig. 4b). In order to understand the drug adsorption mechanism in **I**, we calculated the favorable binding site of 5-FU in the framework of **I**. As shown in Fig. 4c, the snapshot for the 5-FU at zero loading shows that the 5-FU molecule prefers to locate near the $HTATB^{2-}$ ligand with two H-bond interaction observed (N–H and O–H H-bond interactions), and the calculated binding energy is 67 kJ/mol, which is moderate compared to some MOFs for 5-FU loading.

The successful accommodation of 5-FU molecules in the framework of **I** promotes us to study the anticancer activities of the 5-FU loaded **Ia**. In order to explore the low cytotoxicity of the carrier **I**, in vitro cell viabilities of pure compound **I** with various concentrations on the human oral epidermal cells (normal cells) were studied via the MTT assay. As shown in Fig. 5a, the cell viabilities all remained above 80% even at a concentration of 150 μg/mL of **I**, so complex **I** showed low cytotoxicity in the oral epidermal cells. To study the anticancer activity of the 5-FU loaded **Ia** and the compare that with the drug 5-FU, the efficacy of 5-FU loaded **Ia** and 5-FU against were investigated for their ability to eliminate two human lung cancer cells (A549 and NCI-H1299) in 24 and 72 h by cell culture experiment. Based on the results in Fig. 5b, although the number of living cancer cells by **Ia** containing drug is comparable with the free drug in 24 h, it could be observed that the highest cell death (lowest viability) was achieved by the 5-FU loaded **Ia** in 72 h. The above experimental result could be the long-lasting drug release from the 5-FU loaded **Ia**, which could result in improved therapy effect compared with that of using the drug. Similar reported results have also been observed in the literatures [16–20].

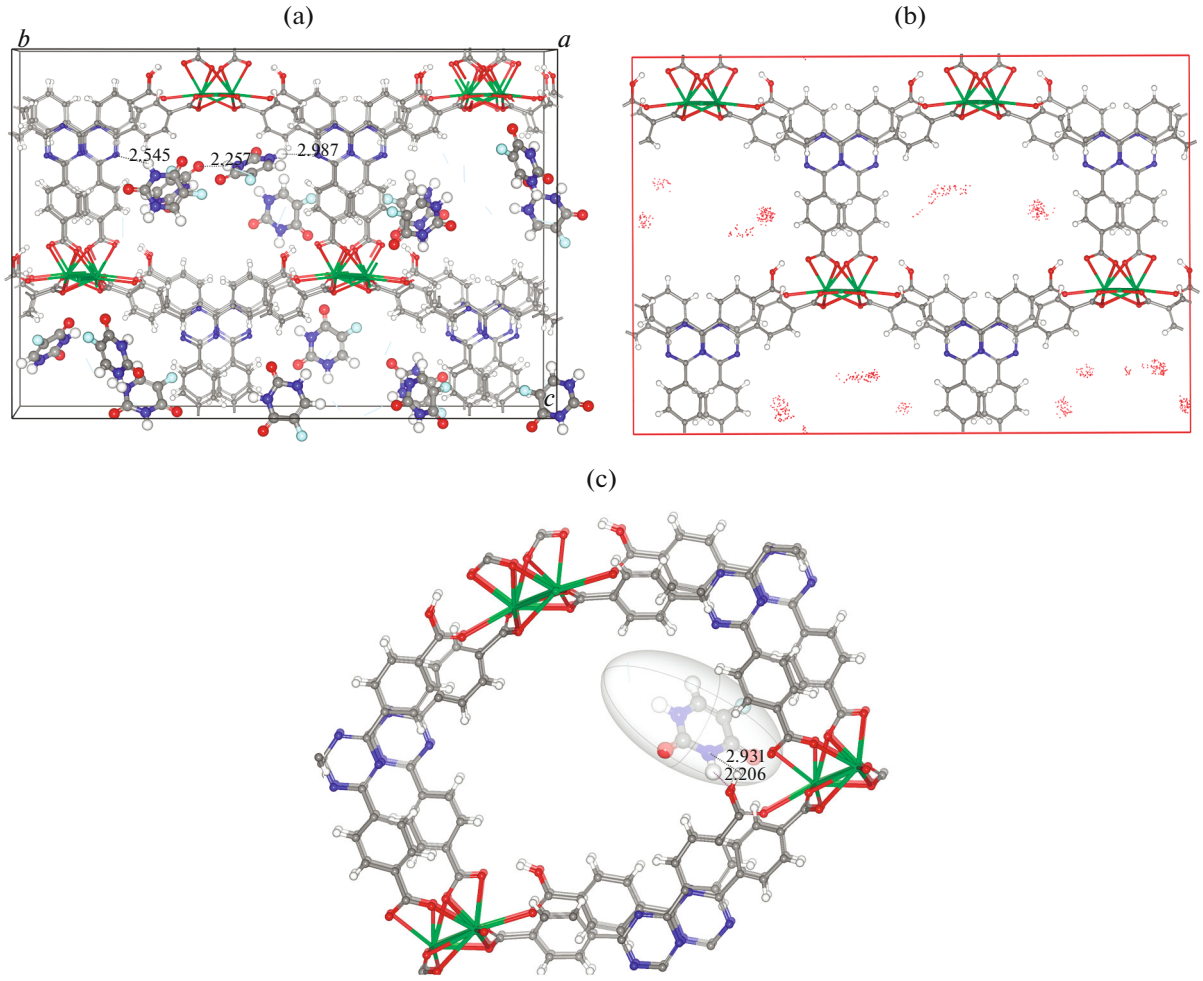

Fig. 4. The conformation of 5-FU in the framework of **I** at 298 K and 1 bar (a); the density of 5-FU in the framework of **I** at saturated loading (b); the favorable binding site of 5-FU in the framework of **I** at zero loading (c).

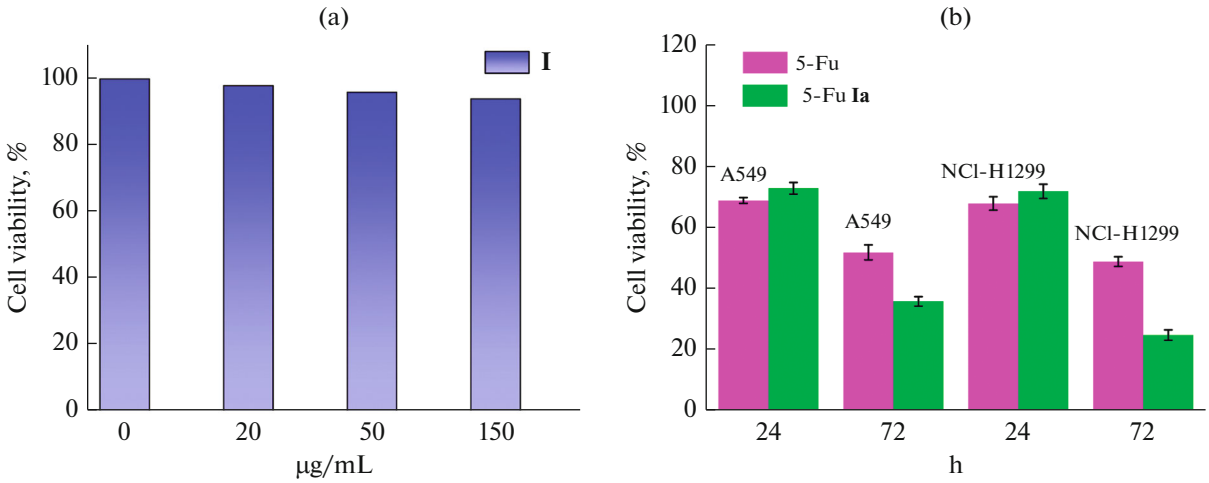

Fig. 5. Cell viabilities of the oral epidermal cells after incubation with **I** at diferent concentrations (a); growth inhibitory effects on A549 and NCI-H1299 cells after 24 and 72 h (b).

REFERENCES

1. Musa, M., Cooperwood, J., and Khan, M.O., *Curr. Med. Chem.*, 2008, vol. 15, p. 2664.
2. Cheng, Q., Li, X., Wang, Y., et al., *Acta Pharmacol. Sin.*, 2018, vol. 39, p. 561.
3. Coates, A., Abraham, S., Kaye, S.B., et al., *Eur. J. Cancer Clin. Oncol.*, 1983, vol. 19, p. 203.
4. Tobin, G., Comby, S., Zhu, N., et al., *Chem. Commun.*, 2015, vol. 51, p. 13313.
5. Chen, D.M., Zhang, N.N., Liu, C.S., et al., *J. Mater. Chem. C.*, 2017, vol. 5, p. 2311.
6. Zhou, H.L., Zhang, Y.B., Zhang, J.P., et al., *Nat. Commun.*, 2015, vol. 6, p. 6917.
7. Li, J., Ji, X.H., and Li, J.T., *J. Mol. Struct.*, 2017, vol. 1147, p. 22.
8. Li, J. and Li, J.T., *Inorg. Chem. Commun.*, 2018, vol. 89, p. 51.
9. Feng, Y., Fan, H., Zhong, Z., et al., *Inorg. Chem.*, 2016, vol. 55, p. 11987.
10. Ke, F., Yuan, Y.P., Qiu, L.G., et al., *J. Mater. Chem.*, 2011, vol. 21, p. 3843.
11. Asha, K.S., Makkitaya, M., Sirohi, A., et al., *CrystEngComm*, 2016, vol. 18, p. 1046.
12. Asha, K.S., Bhattacharjee, R., and Mandal, S., *Angew. Chemie Int. Ed.*, 2016, vol. 55, p. 11528.
13. Foo, M.L., Horike, S., and Kitagawa, S., *Inorg. Chem.*, 2011, vol. 50, p. 11853.
14. Guo, K., Zhao, L., Yu, S., et al., *Inorg. Chem.*, 2018, vol. 57, p. 7104.
15. Dong, X.Y., Hu, X.P., Yao, H.C., et al., *Inorg. Chem.*, 2014, vol. 53, p. 12050.
16. Chen, B., Ma, S., Hurtado, E.J., et al., *Inorg. Chem.*, 2007, vol. 46, p. 8705.
17. Xue, M., Ma, S., Jin, Z., et al., *Inorg. Chem.*, 2008, vol. 47, p. 6825.
18. Miri, B., Motakef-Kazemi, N., Shojaosadati, S.A., et al., *Iran. J. Pharm. Res.*, 2018, vol. 17, p. 1164.
19. Liu, J., Bao, T.Y., Yang, X.Y., et al., *Chem. Commun.*, 2017, vol. 53, p. 7804.
20. Rezaei, M., Abbasi, A., Dinarvand, R., et al., *ACS Appl. Mater. Interfaces*, 2018, vol. 10, p. 17594.